JB Journals.ASM.org

A Cardiolipin-Deficient Mutant of *Rhodobacter sphaeroides* Has an Altered Cell Shape and Is Impaired in Biofilm Formation

Ti-Yu Lin,[a] Thiago M. A. Santos,[a] Wayne S. Kontur,[b,c] Timothy J. Donohue,[b,c] Douglas B. Weibel[a,d,e]

Department of Biochemistry, University of Wisconsin—Madison, Madison, Wisconsin, USA[a]; Department of Bacteriology, University of Wisconsin—Madison, Madison, Wisconsin, USA[b]; DOE Great Lakes Bioenergy Research Center, Madison, Wisconsin, USA[c]; Department of Chemistry, University of Wisconsin—Madison, Madison, Wisconsin, USA[d]; Department of Biomedical Engineering, University of Wisconsin—Madison, Madison, Wisconsin, USA[e]

ABSTRACT

Cell shape has been suggested to play an important role in the regulation of bacterial attachment to surfaces and the formation of communities associated with surfaces. We found that a cardiolipin synthase (Δ*cls*) mutant of the rod-shaped bacterium *Rhodobacter sphaeroides*—in which synthesis of the anionic, highly curved phospholipid cardiolipin (CL) is reduced by 90%—produces ellipsoid-shaped cells that are impaired in biofilm formation. Reducing the concentration of CL did not cause significant defects in *R. sphaeroides* cell growth, swimming motility, lipopolysaccharide and exopolysaccharide production, surface adhesion protein expression, and membrane permeability. Complementation of the CL-deficient mutant by ectopically expressing CL synthase restored cells to their rod shape and increased biofilm formation. Treating *R. sphaeroides* cells with a low concentration (10 μg/ml) of the small-molecule MreB inhibitor *S*-(3,4-dichlorobenzyl)isothiourea produced ellipsoid-shaped cells that had no obvious growth defect yet reduced *R. sphaeroides* biofilm formation. This study demonstrates that CL plays a role in *R. sphaeroides* cell shape determination, biofilm formation, and the ability of the bacterium to adapt to its environment.

IMPORTANCE

Membrane composition plays a fundamental role in the adaptation of many bacteria to environmental stress. In this study, we build a new connection between the anionic phospholipid cardiolipin (CL) and cellular adaptation in *Rhodobacter sphaeroides*. We demonstrate that CL plays a role in the regulation of *R. sphaeroides* morphology and is important for the ability of this bacterium to form biofilms. This study correlates CL concentration, cell shape, and biofilm formation and provides the first example of how membrane composition in bacteria alters cell morphology and influences adaptation. This study also provides insight into the potential of phospholipid biosynthesis as a target for new chemical strategies designed to alter or prevent biofilm formation.

Many bacteria have evolved mechanisms of community-based living based on attachment to surfaces and growth into biofilms. Biofilm formation occurs through several stages. In the first stage, bacterial cells attach to surfaces, replicate, and accumulate to form multilayered cell communities. During biofilm maturation, bacteria secrete a layer of extracellular polymeric substances that encapsulates cells and protects them from environmental stress. At a later stage, planktonic bacterial cells are released into the bulk fluid, attach to new surfaces, replicate, and seed the formation of new biofilms. Biofilms are a central mechanism that bacteria use to adapt to changes in their environment, are prevalent in ecology, and present challenges in industrial applications and medicine due to biofouling and antibiotic resistance (1–3). For example, the North American Centers for Disease Control and Prevention estimates that 65% of all human infections by bacteria involve biofilms (4).

The shape of bacterial cells has been hypothesized to affect their attachment to surfaces and biofilm development (5). During the initial step in biofilm formation, cell attachment requires that the adhesive force between cells and surfaces (measured as 0.31 to 19.6 pN) overcomes the shear force of flowing fluids that are present in many environments (6). On the basis of the mechanisms that cells typically use to attach to surfaces (e.g., fimbriae, flagella, surface adhesion proteins, exopolysaccharides [EPS], and nonspecific, noncovalent forces between the outer membrane lipopolysaccharides [LPSs] and surfaces), cell adhesion has been hypothesized to scale with the surface area available for contact between a cell and surface (5, 7). For bacteria with identical diameters, rod-shaped cells (surface area, 6.28 μm^2) have a larger contact area than spherical cells (surface area, 3.14 μm^2). We hypothesize that rod-shaped bacterial cells attach to surfaces more tightly than sphere-shaped cells by maximizing the contact area and that this leads to an increase in biofilm formation because of a higher initial biomass. This hypothesis is challenging to study because it requires the use of different strains of rod- and sphere-shaped bacteria, which typically have differences in growth rates, cell physiology, and the production of extracellular polymeric substances. In principle, this hypothesis can be studied by using an

Received 23 July 2015 **Accepted** 13 August 2015

Accepted manuscript posted online 17 August 2015

Citation Lin T-Y, Santos TMA, Kontur WS, Donohue TJ, Weibel DB. 2015. A cardiolipin-deficient mutant of *Rhodobacter sphaeroides* has an altered cell shape and is impaired in biofilm formation. J Bacteriol 197:3446–3455. doi:10.1128/JB.00420-15.

Editor: P. de Boer

Address correspondence to Douglas B. Weibel, weibel@biochem.wisc.edu.

Supplemental material for this article may be found at http://dx.doi.org/10.1128/JB.00420-15.

TABLE 1 Bacterial strains and plasmids used in this study

Strain or plasmid	Genotype or description	Source or reference
E. coli strains		
DH5α	*recA1 endA1 gyrA96 thi-1 hsdR17 supE44 relA1 deoR* Δ(*lacZYA-argF*)*U169* λ (ϕ80d*lacZ*ΔM15)	Laboratory collection, CGSC 12384
S17-1	*recA pro hsdR* RP4-2-Tc::Mu-Km::Tn*7*	18
R. sphaeroides strains		
2.4.1	Wild type	ATCC 17023
CL3	2.4.1 with kanamycin resistance cassette in place of genomic *cls*	26
Plasmids		
pIND4	IPTG-inducible expression vector for *R. sphaeroides*, kanamycin resistant	17
pIND4sp	Variant of pIND4 with spectinomycin resistance cassette in place of kanamycin resistance cassette	B. Burger and R. Lemke
pIND5sp	Derivative of pIND4sp with NcoI site replaced with NdeI site	This study
cls-pIND5sp	pIND5sp containing *cls*	This study

organism whose cell shape can be altered without changing key phenotypes that play a central role in biofilm formation.

To test this hypothesis, we turned our attention to *Rhodobacter sphaeroides*. *R. sphaeroides* is a rod-shaped, Gram-negative member of the class *Alphaproteobacteria* that is metabolically diverse and capable of growing in environments where the concentration of salts and nutrients is high, such as soil, mud, sludge, and anoxic zones of waters. *R. sphaeroides* and other *Rhodobacter* species are the primary surface colonists in coastal waters and are known to form biofilms (8, 9). A fascinating characteristic of *R. sphaeroides* is that its cytoplasmic membrane undergoes unusual gymnastics during photosynthetic growth that facilitates the formation of chromatophores, which are the light-harvesting organelles in cells (10). *R. sphaeroides* membranes contain the same three primary classes of phospholipids found in the majority of Gram-negative bacteria: phosphatidylethanolamine, phosphatidylglycerol (PG), and cardiolipin (CL) (11). Bacterial membranes have been historically considered to play a passive role in cell shape determination. For example, CL has been hypothesized to concentrate in regions of large membrane curvature—that is shaped by the peptidoglycan sacculus—to dissipate elastic strain and reduce the membrane free energy (12). The physiological role of CL in *R. sphaeroides* remains largely unexplored, and yet *R. sphaeroides* has been considered a candidate for the origin of mitochondria in which the shape of the inner membrane changes dramatically—as it does in *R. sphaeroides*—and CL is essential (13–15).

In this study, we tested for a previously unrealized connection between CL and cellular adaptation by using *R. sphaeroides*. We demonstrate that a CL-deficient mutant of *R. sphaeroides* has cells with an ellipsoidal shape that are impaired in biofilm formation, particularly in early stages in which cell-to-surface attachment is key. We also show that chemical tools that induce the formation of ellipsoidal cells also produce a defect in biofilm formation. These studies support the hypothesis that rod-shaped bacterial cells attach to surfaces better than sphere-shaped cells do and produce biofilms with higher cell volumes.

MATERIALS AND METHODS

Bacterial strains and growth conditions. *R. sphaeroides* strains were grown aerobically in Sistrom's succinate medium (16) at 30°C with shaking at 200 rpm. When required, ampicillin (50 μg/ml), kanamycin (25 μg/ml), or spectinomycin (5 μg/ml) was added to the medium. *Escherichia coli* strains were grown in LB broth at 37°C with shaking at 200 rpm. When required, ampicillin (50 μg/ml), kanamycin (25 μg/ml), or spectinomycin (50 μg/ml) was added to the medium. The bacterial strains and plasmids used in this study are described in Table 1.

For growth curves, cell cultures in stationary phase were standardized to an absorbance of 1.0 (wavelength of 600 nm). The standardized cultures were inoculated at 1/100 into 1 ml of Sistrom's succinate medium in glass test tubes and grown with shaking for 72 h at 30°C. The absorbance (wavelength of 600 nm) of cell cultures was measured at the time points indicated.

CL synthase expression plasmid (*cls*-pIND5sp) construction. *cls* was amplified by PCR from *R. sphaeroides* 2.4.1 genomic DNA and cloned into pIND5sp at the NdeI and BglII sites by In-Fusion Cloning (Clontech) in accordance with the user manual. The primers used were NdeI-*cls* (5′-GGA GAA ATT AAC ATA TGA TCG ACG ACT GGC TGG GC-3′) and *cls*-BglII (5′-GAT GGT GAT GAG ATC TGA GGT AGC TCT GGA TCG G-3′). pIND5sp is a derivative of pIND4sp (a variant of pIND4 [17] with a spectinomycin resistance cassette) in which the NcoI site was replaced with an NdeI site by using the Stratagene QuikChange XL site-directed mutagenesis kit in accordance with the manufacturer's protocol. The primers used were pIND5sp (5′-GTG ATG GTG ATG AGA TCT GGA TCC TCC ATA TGT TAA TTT CTC CTC TTT AAT TCT AGA TG-3′) and pIND5sp-anti (5′-CAT CTA GAA TTA AAG AGG AGA AAT TAA CAT ATG GAG GAT CCA GAT CTC ATC ACC ATC AC-3′).

Complementation of the CL3 strain. The pIND5sp and *cls*-pIND5sp plasmids were transformed into *E. coli* S17-1 (18) and subsequently mobilized via conjugation into the recipient *R. sphaeroides* wild-type or CL3 strain as described previously (19). The strains harboring these plasmids were incubated for 72 h at 30°C with 1 mM isopropyl-β-D-thiogalactopyranoside (IPTG) to induce expression.

Analysis of cell morphology. An aliquot (4 μl) of cell culture was dropped onto a 2% (wt/vol) agarose pad prepared in phosphate-buffered saline (PBS) buffer (137 mM NaCl, 2.7 mM KCl, 10 mM Na_2HPO_4, 1.76 mM KH_2PO_4, pH 7.4), covered with a glass coverslip, and imaged with an inverted Nikon Eclipse TE2000 microscope equipped with a shuttered black and white Andor iXonEM+ DU-897 electron-multiplying charge-coupled device (EMCCD) camera (Andor Technology, South Windsor, CT). Images were acquired with a 100× objective (Nikon Plan Apo 100×/1.40 oil DM) and the Metamorph software program (version 7.5.6.0; MDS Analytical Technologies, Downingtown, PA). Cell width and length were determined with ImageJ.

Lipid extraction. Polar lipids were extracted from cells by a modified version of the original Bligh-Dyer method (20). Briefly, 50 ml of cell cultures was grown for 72 h at 30°C. Cells were then collected by centrifugation and resuspended in 5 ml of PBS. A 7.5-ml volume of methanol-chloroform (2:1, vol/vol) was added to the cell suspension, and the mixture was shaken for 1 h at 25°C. Two phases were created by adding 2.5 ml

of chloroform and 2.5 ml of 0.1 N HCl and then centrifuging the mixture at 1,000 × *g*, 4°C for 10 min. The bottom chloroform phase was collected with a glass Pasteur pipette and dried under nitrogen in a small glass vial. The extracted lipids were weighed, redissolved in chloroform, and stored at −20°C.

TLC. Total lipid extracts were analyzed by thin-layer chromatography (TLC) on silica gel (TLC silica gel 60, catalog no. HX259108; EMD Millipore). The plate was developed with the solvent chloroform-methanol-acetic acid-water (85:15:10:3.5, vol/vol) (21) and developed in a vapor of iodine until the bands became visible. The CL content was quantified by densitometry with ImageJ. Densitometry was performed without saturation for any phospholipids in the image.

Biofilm formation assays. Static biofilm formation was assayed as described previously (22). Cell cultures in stationary phase were standardized to an absorbance of 1.0 (wavelength of 600 nm). The standardized cultures were inoculated at 1/100 into 100 μl of Sistrom's succinate medium in the wells of a 96-well polystyrene microtiter plate that was then incubated for 72 h at 30°C. Thereafter, the wells were washed with water to remove planktonic cells and biofilms were labeled with 0.1% crystal violet (CV) for 10 min at 25°C. After labeling, the wells were washed with water and the retained CV was solubilized in 30% acetic acid. The amount of biofilm formed in each well was quantified by measuring the absorbance at a wavelength of 550 nm.

To image biofilms, standardized cultures were inoculated at 1/100 into Sistrom's succinate medium containing 5 μg/ml Nile Red in a chamber slide with hydrophobic plastic surfaces (ibidi, Verona, WI) that was then incubated for 72 h at 30°C. After being washed with water, biofilms were imaged on an inverted Nikon Eclipse TE2000 epifluorescence microscope equipped with a shuttered black and white Andor iXonEM+ DU-897 EMCCD camera (Andor Technology, South Windsor, CT). Images were acquired with a 40× objective (Nikon Plan Fluor ELWD 40×/0.60 DM) and the Metamorph software program (version 7.5.6.0; MDS Analytical Technologies, Downingtown, PA).

Imaging of bacterial cell attachment to surfaces. Stationary-phase cell cultures were standardized to an absorbance of 1.0 (wavelength of 600 nm). The standardized cultures were inoculated at 1/100 (~1.25×10^7 cells) into Sistrom's succinate medium in a chamber slide with hydrophobic plastic surfaces (ibidi, Verona, WI) and then incubated at 30°C. Cells attached to the surface were imaged at 1, 24, 48, and 72 h after inoculation. Images were acquired as described in the previous paragraph.

Motility assays. Cell cultures in stationary phase were standardized to an absorbance of 1.0 (wavelength of 600 nm). Five-microliter samples of the standardized cultures were placed on the surfaces of plates containing Sistrom's minimal medium with 0.25% agar (23). Diameters of swimming colonies were measured after incubation for 72 h at 30°C.

Cell velocity measurements. Cell cultures in stationary phase were diluted 1/100 in Sistrom's succinate medium, and a 20-μl aliquot of the diluted suspension was placed inside a ring of Apiezon M grease on precleaned glass slides and sealed with a 1.5-mm glass coverslip. We imaged cell motility with a Nikon Eclipse 80i phase-contrast upright microscope and a black and white Andor LucaS EMCCD camera (Andor Technology). Images were acquired with a 40× ELWD dry objective (Nikon Plan Fluor 40/0.60 dry Ph2 DM). We collected videos consisting of 300 frames with a 33-ms exposure time at a rate of 30 frames/s. Microscopy data were analyzed with MATLAB (MathWorks) by identifying the center of mass of each bacterium in successive frames and grouping those points together to create a cell trajectory from which we determined the mean cell velocity. We used only tracks that had more than 30 frames (i.e., more than 1 s), a minimal total length of 10 μm, and a minimal displacement of 5 μm. Cells that moved in a constant tumbling or wobbling manner or stuck to the coverslip were discarded from the analysis.

qPCRs. Cells were grown to log phase, and RNA was isolated as previously described (24). The RNA samples were then treated with RNase-free DNase (Qiagen, Valencia, CA) and further purified with an RNeasy CleanUp kit (Qiagen, Valencia, CA). cDNA synthesis was performed with a High Capacity RNA-to-cDNA kit (Applied Biosystems, Foster City, CA). Five nanograms of cDNA was used for each quantitative PCR (qPCR). The Applied Biosystems 7500 real-time PCR system (Applied Biosystems, Foster City, CA) with SYBR green chemistry was used to monitor amplification and to quantify the amounts of PCR products. Relative quantitation of gene expression was calculated by the $\Delta\Delta C_T$ method, in which the level of *rpoZ* gene (encodes the Ω subunit of RNA polymerase) expression was used as an internal control. The primers used were *rpoZ* forward (5′-TGA CAA GAA CCC TGT CGT G-3′), *rpoZ* reverse (5′-GCA GCT TCT CTT CGG ACA T-3′), *fliC* forward (5′-CTG ATT GAG ACC CAT GAC CT-3′), *fliC* reverse (5′-GTG AAC GAC CAG TTC AAC AC-3′), *fdp* forward (5′-GAG ATC GAC ACG CCA TTC A-3′), and *fdp* reverse (5′-ACC GAG ATC CTG ACC TAT CA-3′).

LPS extraction. LPS was extracted as described previously (25). Briefly, cell cultures in stationary phase were standardized to an absorbance of 1.0 (wavelength of 600 nm). A 1.5-ml volume of the standardized culture was then collected by centrifugation and resuspended in 200 μl of sodium dodecyl sulfate (SDS) buffer (2% β-mercaptoethanol, 2% SDS, and 10% glycerol in 50 mM Tris-HCl, pH 6.8). Bacteria were boiled for 15 min and treated with proteinase K at 59°C for 3 h. A 200-μl volume of ice-cold Tris-saturated phenol was added to the sample, and the mixture was incubated at 65°C for 15 min with occasional vortexing. A 1-ml volume of diethyl ether was added to the mixture, and two phases were created by centrifugation at 16,100 × *g* for 10 min. The bottom layer containing LPS was collected, mixed with 200 μl of 2× SDS buffer, and run on a 12% SDS-polyacrylamide gel. LPS was visualized by silver staining, and quantitation of LPS content was performed with ImageJ.

EPS extraction. Cell cultures in stationary phase were standardized to an absorbance of 1.0 (wavelength of 600 nm). The standardized cultures were inoculated at 1/100 into 1 ml of Sistrom's succinate medium in glass test tubes that were incubated for 72 h at 30°C with shaking. The cell cultures were centrifuged at 10,000 × *g* for 20 min, and the supernatants were mixed with 3 volumes of absolute ethanol and incubated for 2 h at −20°C to precipitate EPS. The precipitates were collected by centrifugation at 3,000 × *g* for 30 min, washed once with 75% ethanol, and dried at room temperature overnight. The precipitated EPS was dissolved in water, separated by electrophoresis on a 12% SDS-polyacrylamide gel, and visualized by silver staining. Quantitation of the EPS content was performed with ImageJ.

Measurement of membrane permeability by fluorescence microscopy. Samples (0.5 ml) of *R. sphaeroides* cell cultures in stationary phase were collected, concentrated by centrifugation, and resuspended in 0.5 ml of 0.85% NaCl. Propidium iodide (PI) at a final concentration of 20 μM was added to the cell suspension, and samples were incubated for 10 min at 25°C. An aliquot (4 μl) of the cell suspension was imaged as described in the previous section. Measurement of the fluorescence intensity of each cell was performed with ImageJ.

A22 treatment. Cell cultures in stationary phase were standardized to an absorbance of 1.0 (wavelength of 600 nm). The standardized cultures were inoculated at 1/100 into Sistrom's succinate medium containing 10 μg/ml *S*-(3,4-dichlorobenzyl)isothiourea (referred to as A22) or dimethyl sulfoxide (DMSO) as a solvent control. The cells were grown in glass test tubes for 72 h at 30°C with shaking for cell shape analysis or incubated in polystyrene microtiter plates for 72 h at 30°C for biofilm formation assays.

RESULTS

CL deficiency in *R. sphaeroides* changes the shape of cells. A CL-deficient mutant of *R. sphaeroides* (here referred to as *R. sphaeroides* CL3) was created previously by deletion of the CL synthase (*cls*) gene and produces 90% less CL than wild-type cells (26). We were unable to remove CL from *R. sphaeroides* completely by using genomic tools to identify and knock out potential homologs of CL synthase (see the supplemental material) and instead relied on *R. sphaeroides* strain CL3 for our studies. In contrast to rod-shaped wild-type *R. sphaeroides* cells, CL3 cells were ellipsoidal,

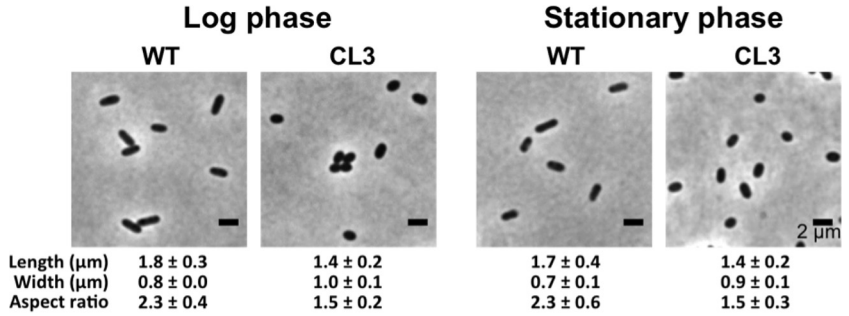

FIG 1 Morphology of *R. sphaeroides* wild-type (WT) and CL3 cells at different growth phases. *R. sphaeroides* WT and CL3 cells were grown aerobically in Sistrom's succinate medium at 30°C with shaking at 200 rpm until they reached log phase (absorbance of ~0.5 at a wavelength of 600 nm) or stationary phase (absorbance of ~1.3 at a wavelength of 600 nm). Each datum point was determined by imaging 300 cells by phase-contrast bright-field microscopy and using ImageJ to determine cell width and length. Shown are mean values ± standard deviations. Differences between the cell shape parameters of the two strains were analyzed by Student's *t* test. The *P* value for all of the parameters measured was <0.001.

had a characteristic decrease (35%) in their aspect ratio (Fig. 1), and yet displayed no significant difference in growth from the wild-type strain (26). We observed the change in *R. sphaeroides* cell shape in both the log and stationary phases, which suggests that this phenotype is growth phase independent.

Complementation of CL synthase in *R. sphaeroides* strain CL3 restores the rod shape of cells. To confirm the role of CL in the change in cell shape that we observed in the CL synthase deletion mutant, we performed a plasmid-based complementation of CL synthase in the CL3 strain. Using TLC analyses, we found that phospholipids extracted from CL3 cells expressing the *R. sphaeroides* CL synthase from plasmid *cls*-pIND5sp contained seven times as much CL as the phospholipids extracted from cells of *R. sphaeroides* CL3 harboring the empty vector pIND5sp (Fig. 2B and C). Complementation of CL biosynthesis in CL3 cells increased the cell aspect ratio by 31% and restored cells to their rod-shaped phenotype (Fig. 2A). These results demonstrate that CL plays a role in the establishment and maintenance of the rod shape of cells of *R. sphaeroides*.

Reducing the concentration of CL alters *R. sphaeroides* biofilm formation. Cell shape has been suggested to play an important role in the attachment of cells to surfaces, in part because the dominant forces of adhesion between cells and surfaces are sensitive to the amount of surface area in contact (5). To investigate the effect of cell shape on the surface attachment and subsequent biofilm development of *R. sphaeroides*, we cultivated biofilms of wild-type and CL3 cells in growth medium containing the cell-permeating, lipophilic fluorescent dye Nile Red. We used Nile Red in these experiments because it labels the cell membrane and makes it possible to visualize cells by epifluorescence/confocal microscopy, is biocompatible, and does not change the cell shape and impede cell growth (27) (see Fig. S1 in the supplemental material). We performed these experiments under static growth conditions (i.e., no flow), which is an ideal system for the study of biofilm formation in early stages in which cell-to-surface attachment is key (22). In addition, static conditions enable us to reproduce and quantify experiments with different *R. sphaeroides* strains. In static cultures, wild-type *R. sphaeroides* cells formed biofilms after 72 h with a mean thickness of 20 μm; however, CL3 cells incubated for 72 h produced only small microcolonies that were 9 μm thick on surfaces and did not form biofilms that extended over larger surface areas (Fig. 3A; see Fig. S2 in the supplemental material). To measure cell-to-surface attachment directly, we imaged surface-attached cells at 1, 24, 48, and 72 h after incubation and counted the cells attached to surfaces at the 1-h time point (Fig. 3B; see Fig. S3 in the supplemental material). Cell adherence was significantly

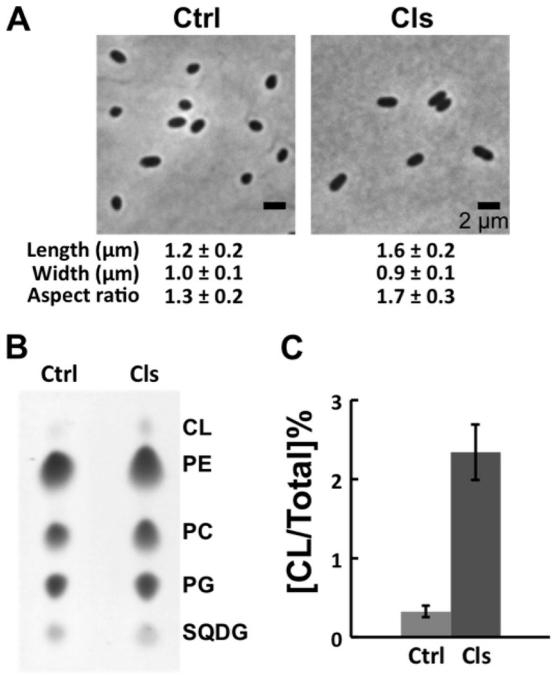

FIG 2 Complementation of the CL3 strain restores the rod shape of cells. (A) Images depicting the morphology of CL3 cells harboring the empty vector pIND5sp (control [Ctrl]) or expressing CL synthase from *cls*-pIND5sp (Cls). Each datum point was determined by imaging 300 cells by phase-contrast bright-field microscopy and using ImageJ to determine cell width and length. Shown are mean values ± standard deviations. Differences between the cell shape parameters of the two strains were analyzed by Student's *t* test. The *P* value for all of the parameters measured was <0.001. (B) TLC analyses of lipids extracted from CL3 cells harboring the empty vector pIND5sp (Ctrl) or expressing CL synthase from *cls*-pIND5sp (Cls). (C) Levels of CL in CL3 cells harboring the empty vector pIND5sp (Ctrl) or expressing CL synthase from *cls*-pIND5sp (Cls). Each datum point was determined from a TLC plate by quantifying the optical densitometry signal with ImageJ. Shown are mean values ± standard deviations obtained from three independent experiments. PE, phosphatidylethanolamine; PC, phosphatidylcholine; SQDG, sulfoquinovosyldiacylglycerol.

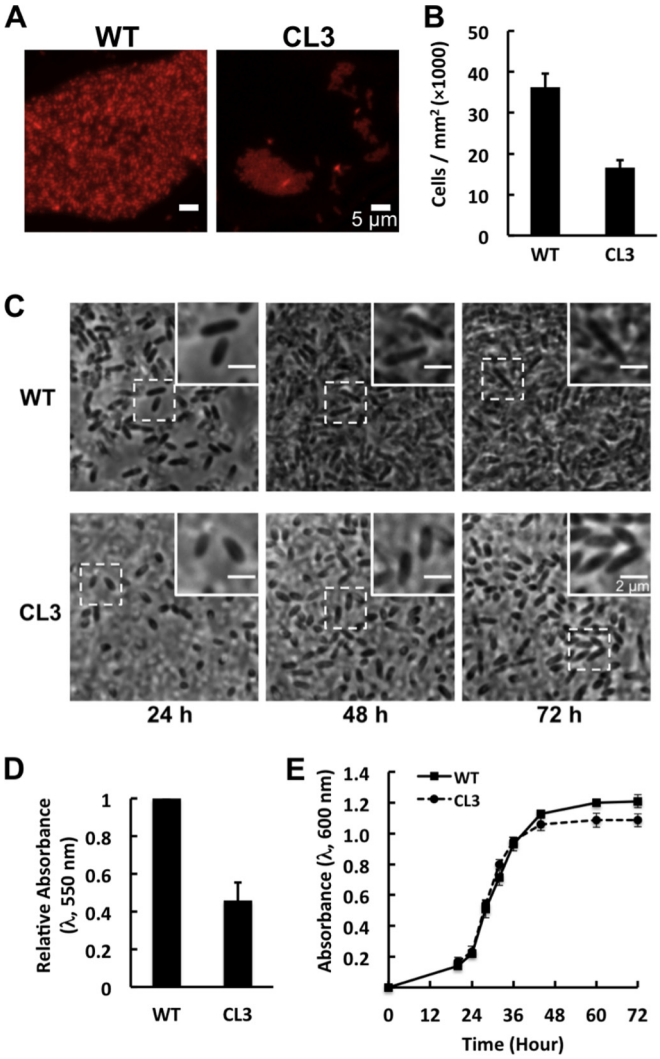

FIG 3 *R. sphaeroides* strain CL3 forms defective biofilms. (A) Representative fluorescence micrographs of *R. sphaeroides* wild-type (WT) and CL3 biofilms grown on a chamber slide with hydrophobic plastic surfaces for 72 h at 30°C in Sistrom's succinate medium containing 5 μg/ml Nile Red. (B and C) *R. sphaeroides* WT and CL3 cells were grown on a chamber slide with hydrophobic plastic surfaces at 30°C in Sistrom's succinate medium. Images were acquired at 1 (see Fig. S3 in the supplemental material), 24, 48, and 72 h after incubation by phase-contrast bright-field microscopy. Insets are magnified views of representative cells that demonstrate changes in cell length. Surface-attached cells were counted at 1 h. Shown are mean values ± standard deviations obtained from three independent experiments. (D) Quantification of *R. sphaeroides* WT and CL3 biofilms grown in wells of a polystyrene microtiter plate for 72 h at 30°C in Sistrom's succinate medium and then labeled with CV. Biofilm formation was quantified by measuring the absorbance of CV at a wavelength of 550 nm. Shown are mean values ± standard deviations obtained from three independent experiments, each performed in eight replicates. (E) Growth curves of *R. sphaeroides* WT and CL3 cells grown with shaking in glass test tubes at 30°C in Sistrom's succinate medium. Shown are mean values ± standard deviations obtained from three independent experiments.

reduced, from $3.6 \times 10^4 \pm 0.3 \times 10^4$ cells/mm^2 in the wild-type strain to $1.7 \times 10^4 \pm 0.2 \times 10^4$ cells/mm^2 in the CL3 mutant (Fig. 3B), suggesting that cells of the *R. sphaeroides* CL3 mutant attached less well to surfaces than wild-type cells did. We observed that wild-type cells increased in length over time when attached to surfaces. CL3 cells that attached to surfaces changed in shape and length from an ellipsoid to a rod shape (Fig. 3C). To quantify early stages of biofilm formation in which biofilm differences may be most pronounced because of the potential impact of cell shape on surface attachment, we cultivated biofilms for 72 h in microtiter dishes with polystyrene surfaces and labeled cells with CV. *R. sphaeroides* strain CL3 displayed a 54% reduction in biofilm formation compared with the wild-type strain after 72 h of incubation (Fig. 3D), which was material independent and occurred on both polystyrene and glass surfaces (see Fig. S4 in the supplemental material). Figure 3E demonstrates that there is no significant difference in planktonic growth between wild-type and CL3 cells. Although an ~0.1 difference in absorbance (wavelength of 600 nm) was observed at stationary phase, the CFU counts of the wild-type and CL3 strains were not significantly different (wild type, 1.6×10^9 CFU/ml; CL3, 1.5×10^9 CFU/ml), suggesting that impaired biofilm formation was not a result of a growth defect.

CL deficiency in *R. sphaeroides* does not cause defects in swimming motility, LPS production, fasciclin I domain protein (*fdp*) gene expression, EPS production, and membrane permeability. Swimming motility plays an important role in biofilm formation by *R. sphaeroides* and other bacterial species (9, 28–31). It has been hypothesized that motility enables cells to overcome surface repulsion forces, contact surfaces, and adsorb. In close physical proximity to surfaces, flagella make it possible for bacterial cells to adsorb and attach to surfaces (7, 30). To examine whether the CL3 strain has motility defects, we assessed the motility of wild-type and CL3 cells in motility agar. After 72 h of incubation at 30°C, CL3 cells displayed swimming diameters comparable to those of wild-type cells (Fig. 4A and B). In addition, we measured the proportion of motile cells in wild-type and CL3 cell cultures in phase-contrast microscopy videos and found no significant difference (wild type, 4.3% ± 2%; CL3, 4.2% ± 1%). We also measured the velocities of single wild-type and CL3 cells by using a particle-tracking algorithm and found no significant difference between the swimming velocities of cells of the two strains (wild type, 30 ± 4 μm/s; CL3, 29 ± 5 μm/s) (Fig. 4C). To confirm these results, we compared the expression levels of the primary flagellar protein FliC in CL3 and wild-type *R. sphaeroides* cells. Using a real-time qPCR assay, we found no significant difference between the expression levels of the *fliC* gene in wild-type and CL3 cells (Fig. 4D). These results suggest that the reduction in CL3 biofilms was unlikely to be due to defects in motility or flagellum assembly.

LPS has been implicated in the attachment of bacterial cells to surfaces (32–34). The O antigen of LPS controls cell surface hydrophobicity and surface charge and influences the interaction of cells with substrates (35). It is unknown whether alterations in membrane composition—specifically, the reduction in the concentration of CL—have an impact on LPS production. To determine whether the CL3 strain has a defect in LPS production, we extracted and compared the LPSs from wild-type and CL3 cells. The LPSs from both *R. sphaeroides* strains displayed similar banding patterns of O-antigen repeats and were present in similar amounts, as evidenced by quantification of the bands on the gel (Fig. 4E and F). These results suggest that the impaired biofilm formation we observed in the CL3 strain was unlikely to be due to defects in LPS production.

R. sphaeroides Fdp has been suggested to function as a surface adhesion protein. Fdp knockout mutants of *R. sphaeroides* lose the ability to adhere to surfaces and form defective biofilms (36). We

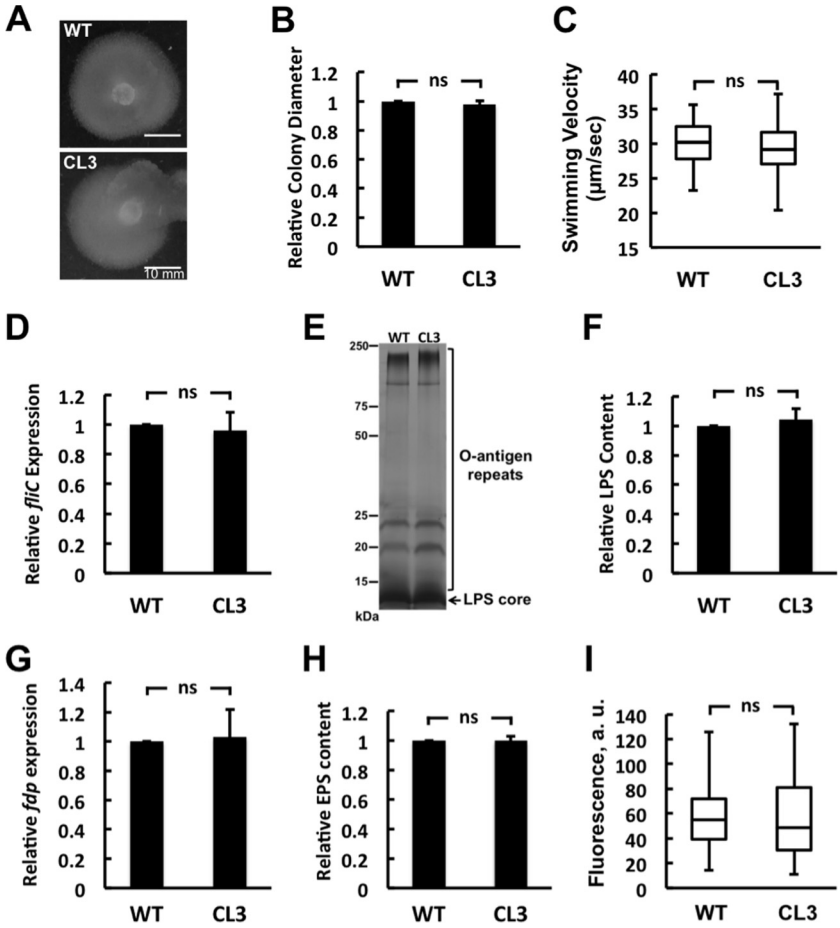

FIG 4 CL deficiency of *R. sphaeroides* does not cause defects in swimming motility, LPS production, *fdp* gene expression, EPS production, and membrane permeability. (A) The motility of the *R. sphaeroides* wild-type (WT) and CL3 strains was assessed by using the same soft-agar swimming plate. (B) Diameters of swimming colonies of the *R. sphaeroides* WT and CL3 strains on soft-agar swimming plates. Shown are mean values ± standard deviations obtained from three independent experiments. (C) Box-and-whisker plots depicting the swimming velocities of individual *R. sphaeroides* WT and CL3 cells ($n = 12$). The extent of the box encompasses the interquartile range of the velocity, whiskers extend to maximum and minimum velocities, and the line within each box represents the median. (D) *fliC* gene expression in *R. sphaeroides* WT and CL3 cells assayed by qPCR. Shown are mean values ± standard deviations obtained from three independent experiments, each performed in triplicate. (E) LPSs from *R. sphaeroides* WT and CL3 cells separated on an SDS-polyacrylamide gel and visualized by silver staining. (F) The LPS content of cells was quantified by densitometry with ImageJ. Shown are mean values ± standard deviations obtained from three independent experiments. (G) *fdp* gene expression in *R. sphaeroides* WT and CL3 cells assayed by qPCR. Shown are mean values ± standard deviations obtained from three independent experiments, each performed in triplicate. (H) The distribution of EPS extracted from planktonic cultures of *R. sphaeroides* WT and CL3 cells, separated on an SDS-polyacrylamide gel, and quantified by densitometry with ImageJ. Shown are mean values ± standard deviations obtained from three independent experiments. (I) Box-and-whisker plots depicting the membrane permeability of the *R. sphaeroides* WT and CL3 strains measured by PI staining ($n \geq 100$). The extent of the box encompasses the interquartile range of the PI fluorescence intensity, whiskers extend to maximum and minimum fluorescence intensities, and the line within each box represents the median. Differences between the parameters of the *R. sphaeroides* WT and CL3 strains were analyzed by Student's *t* test. The *P* value for all of the parameters measured was >0.5. ns, not significant.

compared the transcription levels of the *fdp* gene in the *R. sphaeroides* wild-type and CL3 strains and found no significant difference in *fdp* transcription between wild-type and CL3 cells (Fig. 4G). These results indicate that impaired CL3 biofilm formation is not attributable to changes in Fdp production.

EPS is a key component of the extracellular polymeric substances produced by many biofilm-forming bacteria and required for cellular attachment to surfaces and subsequent biofilm formation (37). To investigate whether the CL3 mutant has defects in EPS production, we extracted EPS from planktonic cultures of wild-type and CL3 cells and analyzed them on an SDS-polyacrylamide gel (see Fig. S5 in the supplemental material). EPS produced from the both *R. sphaeroides* strains was present in similar amounts, as evidenced by quantification of the EPS in the gel (Fig. 4H). These results suggest that the reduction in CL3 biofilms is unlikely to be due to defects in EPS production.

Membrane permeability is connected to a variety of different processes in the cell, including the transport of nutrients, ions and charged molecules, and quorum-sensing compounds. Transport properties have been shown to alter biofilm formation in many bacterial species (38, 39). For example, bacterial quorum sensing is important for the construction of biofilms and the membrane permeability of biofilm cells may play a role in the release of quorum-sensing signals required for biofilm development (38–40). To investigate whether a CL deficiency alters membrane permeability, we used PI, which labels the DNA of cells with disrupted

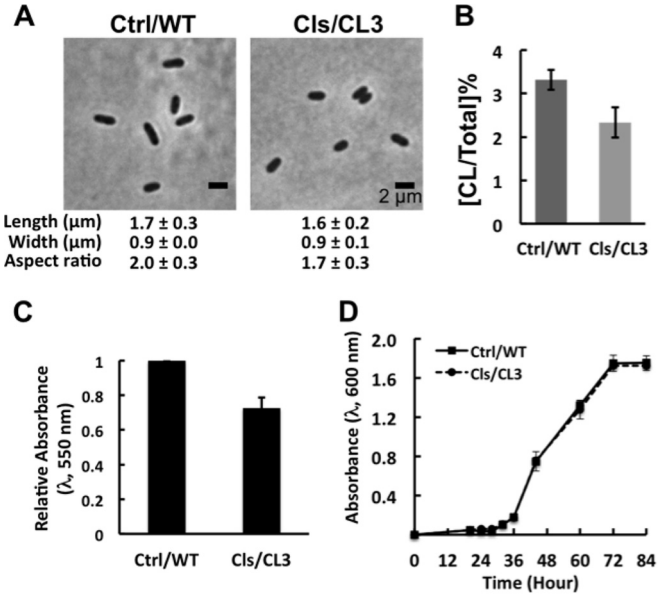

FIG 5 Complementation of the CL3 strain restores biofilm formation. (A) Images depicting the morphology of *R. sphaeroides* wild-type (WT) cells harboring the empty vector pIND5sp (Ctrl/WT) and CL3 cells expressing CL synthase from *cls*-pIND5sp (Cls/CL3). Each datum point was determined by imaging 300 cells by phase-contrast bright-field microscopy and using ImageJ to determine cell width and length. Shown are mean values ± standard deviations. (B) Levels of CL in *R. sphaeroides* WT cells harboring the empty vector pIND5sp (Ctrl/WT) and CL3 cells expressing CL synthase from *cls*-pIND5sp (Cls/CL3). Each datum point was determined from a TLC plate by densitometry with ImageJ. Shown are mean values ± standard deviations obtained from three independent experiments. (C) Quantification of biofilms formed by *R. sphaeroides* WT cells harboring the empty vector pIND5sp (Ctrl/WT) and CL3 cells expressing CL synthase from *cls*-pIND5sp (Cls/CL3). Biofilms were grown on a polystyrene microtiter plate for 72 h at 30°C in Sistrom's succinate medium and then stained with CV. The extent of biofilm formation was determined by measuring the absorbance of CV at a wavelength of 550 nm. Shown are mean values ± standard deviations obtained from three independent experiments, each performed in eight replicates. (D) Growth curves of *R. sphaeroides* WT cells harboring the empty vector pIND5sp (Ctrl/WT) and CL3 cells expressing CL synthase from *cls*-pIND5sp (Cls/CL3). Cells were grown in Sistrom's succinate medium in glass test tubes at 30°C with shaking. Shown are mean values ± standard deviations obtained from three independent experiments.

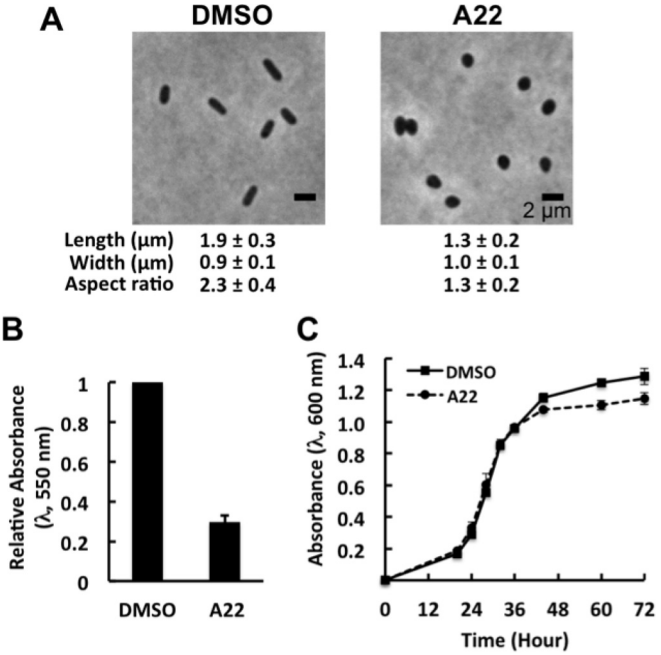

FIG 6 A22 treatment impairs biofilm formation. (A) Images depicting the morphology of *R. sphaeroides* wild-type (WT) cells treated with DMSO or 10 μg/ml A22. Each datum point was determined by imaging 300 cells by phase-contrast bright-field microscopy and using ImageJ to determine cell width and length. Shown are mean values ± standard deviations. Differences between the cell shape parameters of the two treatments were analyzed by Student's *t* test. The *P* value for all of the parameters measured was <0.001. (B) Quantification of biofilms formed by *R. sphaeroides* WT cells treated with DMSO or 10 μg/ml A22. Biofilms were grown in Sistrom's succinate medium containing DMSO or 10 μg/ml A22 on a polystyrene microtiter plate for 72 h at 30°C and then stained with CV. The extent of biofilm formation was determined by measuring the absorbance of CV at a wavelength of 550 nm. Shown are mean values ± standard deviations obtained from three independent experiments, each performed in eight replicates. (C) Growth curves of *R. sphaeroides* WT cells treated with DMSO or 10 μg/ml A22. Cells were grown in Sistrom's succinate medium containing DMSO or 10 μg/ml A22 in glass test tubes at 30°C with shaking. Shown are mean values ± standard deviations obtained from three independent experiments.

membranes. We found that *R. sphaeroides* wild-type and CL3 cells displayed comparable PI fluorescence intensities (Fig. 4I), suggesting that a CL deficiency does not alter membrane integrity and that altered biofilm formation in CL3 was unlikely to be due to defects in membrane permeability.

***R. sphaeroides* cell shape impacts biofilm formation.** To further evaluate whether cell shape regulates biofilm formation, we quantified the effect of CL complementation on the ability of CL3 cells to form biofilms. We expressed *R. sphaeroides* CL synthase from plasmid *cls*-pIND5sp in CL3 cells and the empty vector pIND5sp in wild-type cells. Complementation of CL biosynthesis in CL3 cells increased the cell aspect ratio by 20% compared to that of wild-type cells harboring the empty vector (Fig. 5A). TLC analyses of lipids showed that complementation increased the amount of CL by 60% in CL3 cells compared to that in wild-type cells harboring the empty vector (Fig. 5B). The two strains (CL3 containing *cls*-pIND5sp and the wild type containing pIND5sp) showed no difference in planktonic growth (Fig. 5D). *R. sphaeroides* strain CL3 containing *cls*-pIND5sp restored biofilm formation by 26% (measured by CV labeling) compared to that of wild-type cells (compare Fig. 5C and 3D).

We used a chemical biological approach to independently test if a change in cell shape could cause altered formation of *R. sphaeroides* biofilms. A22 is a small molecule that disrupts the MreB cytoskeleton, causes MreB filaments to depolymerize, and creates rounded cells in many species of bacteria (41, 42). *R. sphaeroides* cells treated with A22 at a concentration of 10 μg/ml (we found that the MIC for *R. sphaeroides* is 60 μg/ml) became round (Fig. 6A); however, no significant changes in planktonic growth were observed over 72 h of growth (Fig. 6C). Although A22 treatment caused a decrease in absorbance (wavelength of 600 nm) of ~0.1 at stationary phase, it did not significantly reduce the number of viable cells present (DMSO control, 1.7×10^9 CFU/ml; A22, 1.6×10^9 CFU/ml). The alteration in *R. sphaeroides* cell shape due to A22 treatment caused a 70% reduction in biofilm formation (measured by CV labeling) compared to that of wild-type cells (Fig. 6B). These results confirm our observation that CL influences *R. sphaeroides* cell shape and affects biofilm formation.

DISCUSSION

CL plays an essential role in the adaptation of many bacterial species to environmental stresses, including high salinity and low pH (43–46). CL has also been reported to play an important role in the regulation of essential processes in bacteria, including cell division, ATP synthesis, and protein translocation across membranes (47–50). Remarkably little is known about the function of CL in *R. sphaeroides*. The interaction of *R. sphaeroides* cytochrome *c* oxidase (C*c*O) and CL is essential for the full activity of the enzyme (51–54). However, a previous study demonstrated that a CL deficiency in *R. sphaeroides* does not impair the structure and function of C*c*O or cause any significant growth defects (26). Several groups have demonstrated that PG can override the absence of CL in *E. coli* and restore the interaction of proteins with the membrane, which may explain the results of those previous studies with *R. sphaeroides* C*c*O (55–57).

In *E. coli*, three *cls* genes have been identified; *clsA*, *clsB*, and *clsC* show DNA sequence homology and belong to the phospholipase D superfamily. Strains with the individual genes knocked out still produce some CL; however, triple *cls* knockout *E. coli* strain BKT12 does not produce any detectable CL (58). To remove CL completely from *R. sphaeroides* cells, we used computational tools to identify homologous genes that code for other CL synthases. Our analysis identified the phospholipase D family protein RSP_0113, which may be responsible for the residual CL in the CL3 strain (see the supplemental material). However, we found that RSP_0113 does not catalyze the synthesis of CL in *R. sphaeroides*, as ectopically expressing it in the CL3 strain did not change the relative concentration of CL present. We are unsure of the origins of the residual CL in *R. sphaeroides* strain CL3, which may come from the promiscuity of another phospholipid synthase, such as phosphatidylserine synthase, as has been reported in other cells (26).

Although the CL3 strain shows no significant defects in growth, it exhibits a characteristic ellipsoidal cell shape phenotype in both the log and stationary phases. Rod-shaped bacteria can undergo a similar morphological change when the rate of cell division is higher than the rate of cell mass production. The CL3 strain has a division rate (Fig. 3E) (26) and a cell volume (~1.3 μm^3) similar to those of the wild-type strain (~1.2 μm^3), which suggests that the alteration in its shape is not due to a change in cell volume or decoupling of growth rate and division. As cells of *E. coli* and many other rod-shaped bacterial species enter stationary phase, they often adopt a sphere-like morphology (59, 60). We did not observe a similar growth phase-dependent change in wild-type *R. sphaeroides* cell shape (i.e., cells remain rod shaped). Our results are consistent with a change in the shape of cells of the CL3 strain that is not related to growth conditions.

Bacterial cell shape has been hypothesized to play an important role in the regulation of the attachment of cells to surfaces, which occurs at early stages of biofilm formation. Cell shape determines the amount of the cell body in contact with surfaces and has been suggested to regulate subsequent biofilm development (5). We hypothesized that a CL deficiency in *R. sphaeroides* can cause a reduction in biofilm formation (compared to that of wild-type cells), as the ellipsoidal cells have a reduced surface area that limits surface attachment. Bacterial cell length and curvature are primary determinants for maximization of the amount of contact between bacterial cells and surfaces. Because of our inability to measure mean cell curvature accurately, we do not include a formal analysis of the effect of curvature on cell attachment; however, papers in other areas of biology have described the connection between cell curvature and maximization of surface contact (61). To test the hypothesis regarding *R. sphaeroides* cell geometry and surface attachment, we compared biofilms of wild-type and CL3 *R. sphaeroides* strains grown in static cultures. Static growth conditions do not promote the biofilm maturation typically associated with flow cell systems and are effective at identifying factors required for cell-to-surface attachment (22). *R. sphaeroides* strain CL3 displayed weaker attachment to surfaces than the wild-type strain and formed defective biofilms, which is consistent with the observation that a *rodA* mutant of *Burkholderia cepacia* forms spherical cells and shows impaired biofilm formation (62). The hypothesis that bacteria can increase the strength of their attachment to surfaces by altering their cell shape has been proposed previously (e.g., a rod-shaped cell elongating into a filament and a spherical cell increasing its length and becoming rod shaped) yet has not been tested (5). We found that cells of both the wild-type and CL3 *R. sphaeroides* strains increase in length when attached to surfaces, suggesting that they may be maximizing surface contact.

Cell shape also plays a role in the regulation of bacterial motility, which is important for the initial attachment of cells to surfaces and subsequent biofilm development (29, 63). We found that a CL deficiency in *R. sphaeroides* alters cell shape but not swimming motility, which is interesting. However, the *R. sphaeroides* cell is unlike that of most rod-shaped bacteria in terms of the location of its individual flagellum (not polar like most bacteria) and its biophysics and motility mechanism. Consequently, much of what we know about the influence of the shape of bacterial cells on their motility may not be applicable to *R. sphaeroides*.

LPS is the major component of the outer membrane of Gram-negative bacteria and has been shown to regulate cell attachment to surfaces (32–35). Fdp is a surface adhesion protein that is localized at the inner membranes of *R. sphaeroides* and facilitates the attachment of cells to surfaces and thus the development of biofilms (36). EPS is important for cell-to-surface attachment and is often referred to as a primary glue or cement for biofilms (37). Our data indicate that the CL3 strain is not defective in any of these primary factors for initiation of biofilm formation. A CL deficiency may cause a change in the anionic composition of membranes that affects the surface charge of cells and their attachment to surfaces. However, the level of PG is increased in the CL3 mutant and thereby retains the negatively charged character of membranes (26).

Quorum sensing occurs between cells in biofilms and signals biofilm development in several species of bacteria (38). Changes in bacterial membrane permeability could alter quorum sensing—and a variety of other cellular processes that are influenced by changes in molecular transport into the cell—and affect biofilm formation. We found that the membrane permeability of CL3 cells is unchanged (compared to that of wild-type cells). *R. sphaeroides* produces acylhomoserine lactone, a quorum-sensing signal that regulates EPS production (64). Since CL3 cells produce an amount of EPS similar to that of wild-type cells, it is unlikely that the quorum-sensing system is impaired in CL3 biofilms. These data suggest that a change in cell shape caused by CL deficiency is the primary factor that impairs biofilm formation by the *R. sphaeroides* CL3 strain, and not other physiological consequences that accompany a change in cell shape.

To further evaluate whether cell shape regulates biofilm formation, we quantified the effect of CL complementation on the ability of the CL3 strain to form biofilms and found that it restored a rod-shaped morphology and recovered its ability to form biofilms. Complementation was unable to completely recover biofilm formation by the CL3 strain, which we attribute to our inability to restore native levels of CL and completely recover the rod shape of CL3 cells. These results correlate the CL concentration to the cell shape and biofilm formation.

MreB is a bacterial cytoskeletal protein that is homologous to eukaryotic actin (65). In rod-shaped bacteria, MreB polymerizes into dynamic filaments that move circumferentially around the cytoplasmic membrane of cells, interacts with cell wall synthesis machinery, and plays a role in the maintenance of cell shape (66–68). A22 is a small-molecule inhibitor that binds MreB, disassembles filaments, causes the protein to mislocalize in cells, and produces cells with a spherical shape (41, 42). Treatment of *R. sphaeroides* cells with A22 produced round cells and suggests that the MreB-mediated rod shape formation model in many Gram-negative bacteria is conserved in *R. sphaeroides*. We quantified the effect of low concentrations of A22 on *R. sphaeroides* cells and found that it produced spherical cells, did not alter cell growth, and reduced biofilm formation similar to our experiments reducing CL.

In conclusion, we have demonstrated that conditions that alter *R. sphaeroides* cell shape (a CL deficiency or a compound that blocks MreB activity) impede its ability to form biofilms. We suggest that cell shape affects biofilm formation by reducing the surface area available for cell attachment to surfaces. The *R. sphaeroides* CL3 mutant is the first example that we are aware of in which the cell membrane composition alters cell morphology and influences the bacterium's adaptation by reducing the ability to form multicellular structures. Future studies will extend these results to other bacteria and explore the molecular mechanisms that connect CL to bacterial cell shape.

ACKNOWLEDGMENTS

We thank the Ferguson-Miller laboratory (Michigan State University) for strain CL3 and the Raetz laboratory (Duke University) for strain BKT12. We thank Brian Burger and Rachelle Lemke for constructing and providing pIND4sp. This project leveraged technical assistance and input from George Auer, Manohary Rajendram, Julia Nepper, and Piercen Oliver.

T.-Y. Lin acknowledges a William H. Peterson fellowship from the Department of Biochemistry, University of Wisconsin—Madison. The National Science Foundation (MCB-1120832 and DMR-1121288), NIH (1DP2OD008735), USDA (WIS01594), and Department of Energy Office of Science (BER DE-FC02-07ER64494) supported this research.

REFERENCES

1. **Garrett TR, Bhakoo M, Zhang Z.** 2008. Bacterial adhesion and biofilms on surfaces. Prog Nat Sci **18:**1049–1056. http://dx.doi.org/10.1016/j.pnsc.2008.04.001.
2. **Dunne WM.** 2002. Bacterial adhesion: seen any good biofilms lately? Clin Microbiol Rev **15:**155–166. http://dx.doi.org/10.1128/CMR.15.2.155-166.2002.
3. **Renner LD, Weibel DB.** 2011. Physicochemical regulation of biofilm formation. MRS Bull **36:**347–355. http://dx.doi.org/10.1557/mrs.2011.65.
4. **Potera C.** 1999. Forging a link between biofilms and disease. Science **283:**1837–1839. http://dx.doi.org/10.1126/science.283.5409.1837.
5. **Young KD.** 2006. The selective value of bacterial shape. Microbiol Mol Biol Rev **70:**660–703. http://dx.doi.org/10.1128/MMBR.00001-06.
6. **Boks NP, Norde W, van der Mei HC, Busscher HJ.** 2008. Forces involved in bacterial adhesion to hydrophilic and hydrophobic surfaces. Microbiology **154:**3122–3133. http://dx.doi.org/10.1099/mic.0.2008/018622-0.
7. **Tuson HH, Weibel DB.** 2013. Bacteria-surface interactions. Soft Matter **9:**4368–4380. http://dx.doi.org/10.1039/c3sm27705d.
8. **Dang H, Lovell CR.** 2002. Numerical dominance and phylotype diversity of marine *Rhodobacter* species during early colonization of submerged surfaces in coastal marine waters as determined by 16S ribosomal DNA sequence analysis and fluorescence in situ hybridization. Appl Environ Microbiol **68:**496–504. http://dx.doi.org/10.1128/AEM.68.2.496-504.2002.
9. **Wilkinson DA, Chacko SJ, Venien-Bryan C, Wadhams GH, Armitage JP.** 2011. Regulation of flagellum number by FliA and FlgM and role in biofilm formation by *Rhodobacter sphaeroides*. J Bacteriol **193:**4010–4014. http://dx.doi.org/10.1128/JB.00349-11.
10. **Chory J, Donohue TJ, Varga AR, Staehelin LA, Kaplan S.** 1984. Induction of the photosynthetic membranes of *Rhodopseudomonas sphaeroides*: biochemical and morphological studies. J Bacteriol **159:**540–554.
11. **Russell NJ, Harwood JL.** 1979. Changes in the acyl lipid composition of photosynthetic bacteria grown under photosynthetic and non-photosynthetic conditions. Biochem J **181:**339–345. http://dx.doi.org/10.1042/bj1810339.
12. **Huang KC, Mukhopadhyay R, Wingreen NS.** 2006. A curvature-mediated mechanism for localization of lipids to bacterial poles. PLoS Comput Biol **2:**e151. http://dx.doi.org/10.1371/journal.pcbi.0020151.
13. **Woese CR.** 1987. Bacterial evolution. Microbiol Rev **51:**221–271.
14. **Yeliseev AA, Krueger KE, Kaplan S.** 1997. A mammalian mitochondrial drug receptor functions as a bacterial "oxygen" sensor. Proc Natl Acad Sci U S A **94:**5101–5106. http://dx.doi.org/10.1073/pnas.94.10.5101.
15. **Mileykovskaya E, Dowhan W.** 2009. Cardiolipin membrane domains in prokaryotes and eukaryotes. Biochim Biophys Acta **1788:**2084–2091. http://dx.doi.org/10.1016/j.bbamem.2009.04.003.
16. **Sistrom WR.** 1960. A requirement for sodium in the growth of *Rhodopseudomonas spheroides*. J Gen Microbiol **22:**778–785. http://dx.doi.org/10.1099/00221287-22-3-778.
17. **Ind AC, Porter SL, Brown MT, Byles ED, de Beyer JA, Godfrey SA, Armitage JP.** 2009. Inducible-expression plasmid for *Rhodobacter sphaeroides* and *Paracoccus denitrificans*. Appl Environ Microbiol **75:**6613–6615. http://dx.doi.org/10.1128/AEM.01587-09.
18. **Simon R, Priefer U, Pühler A.** 1983. A broad host range mobilization system for in vitro genetic engineering: transposon mutagenesis in Gram negative bacteria. Bio-Technology **1:**784–791.
19. **Davis J, Donohue TJ, Kaplan S.** 1988. Construction, characterization, and complementation of a Puf$^-$ mutant of *Rhodobacter sphaeroides*. J Bacteriol **170:**320–329.
20. **Bligh EG, Dyer WJ.** 1959. A rapid method of total lipid extraction and purification. Can J Biochem Physiol **37:**911–917. http://dx.doi.org/10.1139/o59-099.
21. **De Leo V, Catucci L, Ventrella A, Milano F, Agostiano A, Corcelli A.** 2009. Cardiolipin increases in chromatophores isolated from *Rhodobacter sphaeroides* after osmotic stress: structural and functional roles. J Lipid Res **50:**256–264.
22. **O'Toole GA.** 2011. Microtiter dish biofilm formation assay. J Vis Exp **47:**2437. http://dx.doi.org/10.3791/2437.
23. **Suaste-Olmos F, Domenzain C, Mireles-Rodriguez JC, Poggio S, Osorio A, Dreyfus G, Camarena L.** 2010. The flagellar protein FliL is essential for swimming in *Rhodobacter sphaeroides*. J Bacteriol **192:**6230–6239. http://dx.doi.org/10.1128/JB.00655-10.
24. **Tavano CL, Podevels AM, Donohue TJ.** 2005. Identification of genes required for recycling reducing power during photosynthetic growth. J Bacteriol **187:**5249–5258. http://dx.doi.org/10.1128/JB.187.15.5249-5258.2005.
25. **Davis MR, Jr, Goldberg JB.** 2012. Purification and visualization of lipopolysaccharide from Gram-negative bacteria by hot aqueous-phenol extraction. J Vis Exp **63:**3916. http://dx.doi.org/10.3791/3916.
26. **Zhang X, Tamot B, Hiser C, Reid GE, Benning C, Ferguson-Miller S.** 2011. Cardiolipin deficiency in *Rhodobacter sphaeroides* alters the lipid profile of membranes and of crystallized cytochrome oxidase, but structure and function are maintained. Biochemistry **50:**3879–3890. http://dx.doi.org/10.1021/bi101702c.
27. **Spiekermann P, Rehm BH, Kalscheuer R, Baumeister D, Steinbuchel A.** 1999. A sensitive, viable-colony staining method using Nile red for direct screening of bacteria that accumulate polyhydroxyalkanoic acids and other lipid storage compounds. Arch Microbiol **171:**73–80. http://dx.doi.org/10.1007/s002030050681.
28. **Merritt PM, Danhorn T, Fuqua C.** 2007. Motility and chemotaxis in

Agrobacterium tumefaciens surface attachment and biofilm formation. J Bacteriol **189:**8005–8014. http://dx.doi.org/10.1128/JB.00566-07.
29. **O'Toole GA, Kolter R.** 1998. Flagellar and twitching motility are necessary for *Pseudomonas aeruginosa* biofilm development. Mol Microbiol **30:**295–304. http://dx.doi.org/10.1046/j.1365-2958.1998.01062.x.
30. **Pratt LA, Kolter R.** 1998. Genetic analysis of *Escherichia coli* biofilm formation: roles of flagella, motility, chemotaxis and type I pili. Mol Microbiol **30:**285–293. http://dx.doi.org/10.1046/j.1365-2958.1998.01061.x.
31. **Anderson JK, Smith TG, Hoover TR.** 2010. Sense and sensibility: flagellum-mediated gene regulation. Trends Microbiol **18:**30–37. http://dx.doi.org/10.1016/j.tim.2009.11.001.
32. **Walker SL, Redman JA, Elimelech M.** 2004. Role of cell surface lipopolysaccharides in *Escherichia coli* K12 adhesion and transport. Langmuir **20:**7736–7746. http://dx.doi.org/10.1021/la049511f.
33. **Abu-Lail NI, Camesano TA.** 2003. Role of lipopolysaccharides in the adhesion, retention, and transport of *Escherichia coli* JM109. Environ Sci Technol **37:**2173–2183. http://dx.doi.org/10.1021/es026159o.
34. **Kannenberg EL, Carlson RW.** 2001. Lipid A and O-chain modifications cause *Rhizobium* lipopolysaccharides to become hydrophobic during bacteroid development. Mol Microbiol **39:**379–391. http://dx.doi.org/10.1046/j.1365-2958.2001.02225.x.
35. **Makin SA, Beveridge TJ.** 1996. The influence of A-band and B-band lipopolysaccharide on the surface characteristics and adhesion of *Pseudomonas aeruginosa* to surfaces. Microbiology **142**(Pt 2):299–307. http://dx.doi.org/10.1099/13500872-142-2-299.
36. **Moody RG, Williamson MP.** 2013. Structure and function of a bacterial fasciclin I domain protein elucidates function of related cell adhesion proteins such as TGFBIp and periostin. FEBS Open Bio **3:**71–77. http://dx.doi.org/10.1016/j.fob.2013.01.001.
37. **Costerton JW, Cheng KJ, Geesey GG, Ladd TI, Nickel JC, Dasgupta M, Marrie TJ.** 1987. Bacterial biofilms in nature and disease. Annu Rev Microbiol **41:**435–464. http://dx.doi.org/10.1146/annurev.mi.41.100187.002251.
38. **Parsek MR, Greenberg EP.** 2005. Sociomicrobiology: the connections between quorum sensing and biofilms. Trends Microbiol **13:**27–33. http://dx.doi.org/10.1016/j.tim.2004.11.007.
39. **Li YH, Tian X.** 2012. Quorum sensing and bacterial social interactions in biofilms. Sensors (Basel) **12:**2519–2538. http://dx.doi.org/10.3390/s120302519.
40. **McDougald D, Rice SA, Barraud N, Steinberg PD, Kjelleberg S.** 2011. Should we stay or should we go: mechanisms and ecological consequences for biofilm dispersal. Nat Rev Microbiol **10:**39–50.
41. **Bean GJ, Flickinger ST, Westler WM, McCully ME, Sept D, Weibel DB, Amann KJ.** 2009. A22 disrupts the bacterial actin cytoskeleton by directly binding and inducing a low-affinity state in MreB. Biochemistry **48:**4852–4857. http://dx.doi.org/10.1021/bi900014d.
42. **Iwai N, Nagai K, Wachi M.** 2002. Novel *S*-benzylisothiourea compound that induces spherical cells in *Escherichia coli* probably by acting on a rod-shape-determining protein(s) other than penicillin-binding protein 2. Biosci Biotechnol Biochem **66:**2658–2662. http://dx.doi.org/10.1271/bbb.66.2658.
43. **López CS, Alice AF, Heras H, Rivas EA, Sanchez-Rivas C.** 2006. Role of anionic phospholipids in the adaptation of *Bacillus subtilis* to high salinity. Microbiology **152:**605–616. http://dx.doi.org/10.1099/mic.0.28345-0.
44. **MacGilvray ME, Lapek JD, Jr, Friedman AE, Quivey RG, Jr.** 2012. Cardiolipin biosynthesis in *Streptococcus mutans* is regulated in response to external pH. Microbiology **158:**2133–2143. http://dx.doi.org/10.1099/mic.0.057273-0.
45. **Tsai M, Ohniwa RL, Kato Y, Takeshita SL, Ohta T, Saito S, Hayashi H, Morikawa K.** 2011. *Staphylococcus aureus* requires cardiolipin for survival under conditions of high salinity. BMC Microbiol **11:**13. http://dx.doi.org/10.1186/1471-2180-11-13.
46. **Romantsov T, Helbig S, Culham DE, Gill C, Stalker L, Wood JM.** 2007. Cardiolipin promotes polar localization of osmosensory transporter ProP in *Escherichia coli*. Mol Microbiol **64:**1455–1465. http://dx.doi.org/10.1111/j.1365-2958.2007.05727.x.
47. **Hsieh CW, Lin TY, Lai HM, Lin CC, Hsieh TS, Shih YL.** 2010. Direct MinE-membrane interaction contributes to the proper localization of MinDE in *E. coli*. Mol Microbiol **75:**499–512. http://dx.doi.org/10.1111/j.1365-2958.2009.07006.x.
48. **Haines TH, Dencher NA.** 2002. Cardiolipin: a proton trap for oxidative phosphorylation. FEBS Lett **528:**35–39. http://dx.doi.org/10.1016/S0014-5793(02)03292-1.
49. **Gold VA, Robson A, Bao H, Romantsov T, Duong F, Collinson I.** 2010. The action of cardiolipin on the bacterial translocon. Proc Natl Acad Sci U S A **107:**10044–10049. http://dx.doi.org/10.1073/pnas.0914680107.
50. **Renner LD, Weibel DB.** 2011. Cardiolipin microdomains localize to negatively curved regions of *Escherichia coli* membranes. Proc Natl Acad Sci U S A **108:**6264–6269. http://dx.doi.org/10.1073/pnas.1015757108.
51. **Wakeham MC, Sessions RB, Jones MR, Fyfe PK.** 2001. Is there a conserved interaction between cardiolipin and the type II bacterial reaction center? Biophys J **80:**1395–1405. http://dx.doi.org/10.1016/S0006-3495(01)76112-7.
52. **McAuley KE, Fyfe PK, Ridge JP, Isaacs NW, Cogdell RJ, Jones MR.** 1999. Structural details of an interaction between cardiolipin and an integral membrane protein. Proc Natl Acad Sci U S A **96:**14706–14711. http://dx.doi.org/10.1073/pnas.96.26.14706.
53. **Distler AM, Allison J, Hiser C, Qin L, Hilmi Y, Ferguson-Miller S.** 2004. Mass spectrometric detection of protein, lipid and heme components of cytochrome *c* oxidase from *R. sphaeroides* and the stabilization of noncovalent complexes from the enzyme. Eur J Mass Spectrom (Chichester, Eng) **10:**295–308. http://dx.doi.org/10.1255/ejms.594.
54. **Svensson-Ek M, Abramson J, Larsson G, Tornroth S, Brzezinski P, Iwata S.** 2002. The X-ray crystal structures of wild-type and EQ(I-286) mutant cytochrome *c* oxidases from *Rhodobacter sphaeroides*. J Mol Biol **321:**329–339. http://dx.doi.org/10.1016/S0022-2836(02)00619-8.
55. **Oliver PM, Crooks JA, Leidl M, Yoon EJ, Saghatelian A, Weibel DB.** 2014. Localization of anionic phospholipids in *Escherichia coli* cells. J Bacteriol **196:**3386–3398. http://dx.doi.org/10.1128/JB.01877-14.
56. **Romantsov T, Guan Z, Wood JM.** 2009. Cardiolipin and the osmotic stress responses of bacteria. Biochim Biophys Acta **1788:**2092–2100. http://dx.doi.org/10.1016/j.bbamem.2009.06.010.
57. **Shibuya I, Miyazaki C, Ohta A.** 1985. Alteration of phospholipid composition by combined defects in phosphatidylserine and cardiolipin synthases and physiological consequences in *Escherichia coli*. J Bacteriol **161:**1086–1092.
58. **Tan BK, Bogdanov M, Zhao J, Dowhan W, Raetz CR, Guan Z.** 2012. Discovery of a cardiolipin synthase utilizing phosphatidylethanolamine and phosphatidylglycerol as substrates. Proc Natl Acad Sci U S A **109:**16504–16509. http://dx.doi.org/10.1073/pnas.1212797109.
59. **Kjelleberg S, Hermansson M, Marden P, Jones GW.** 1987. The transient phase between growth and nongrowth of heterotrophic bacteria, with emphasis on the marine environment. Annu Rev Microbiol **41:**25–49. http://dx.doi.org/10.1146/annurev.mi.41.100187.000325.
60. **Lange R, Hengge-Aronis R.** 1991. Growth phase-regulated expression of *bolA* and morphology of stationary-phase *Escherichia coli* cells are controlled by the novel sigma factor sigma S. J Bacteriol **173:**4474–4481.
61. **Persat A, Stone HA, Gitai Z.** 2014. The curved shape of Caulobacter crescentus enhances surface colonization in flow. Nat Commun **5:**3824.
62. **Huber B, Riedel K, Kothe M, Givskov M, Molin S, Eberl L.** 2002. Genetic analysis of functions involved in the late stages of biofilm development in *Burkholderia cepacia* H111. Mol Microbiol **46:**411–426. http://dx.doi.org/10.1046/j.1365-2958.2002.03182.x.
63. **Watnick PI, Kolter R.** 1999. Steps in the development of a Vibrio cholerae El Tor biofilm. Mol Microbiol **34:**586–595. http://dx.doi.org/10.1046/j.1365-2958.1999.01624.x.
64. **Puskas A, Greenberg EP, Kaplan S, Schaefer AL.** 1997. A quorum-sensing system in the free-living photosynthetic bacterium *Rhodobacter sphaeroides*. J Bacteriol **179:**7530–7537.
65. **van den Ent F, Amos LA, Lowe J.** 2001. Prokaryotic origin of the actin cytoskeleton. Nature **413:**39–44. http://dx.doi.org/10.1038/35092500.
66. **Domínguez-Escobar J, Chastanet A, Crevenna AH, Fromion V, Wedlich-Soldner R, Carballido-López R.** 2011. Processive movement of MreB-associated cell wall biosynthetic complexes in bacteria. Science **333:**225–228. http://dx.doi.org/10.1126/science.1203466.
67. **Figge RM, Divakaruni AV, Gober JW.** 2004. MreB, the cell shape-determining bacterial actin homologue, co-ordinates cell wall morphogenesis in *Caulobacter crescentus*. Mol Microbiol **51:**1321–1332. http://dx.doi.org/10.1111/j.1365-2958.2003.03936.x.
68. **Reimold C, Defeu Soufo HJ, Dempwolff F, Graumann PL.** 2013. Motion of variable-length MreB filaments at the bacterial cell membrane influences cell morphology. Mol Biol Cell **24:**2340–2349. http://dx.doi.org/10.1091/mbc.E12-10-0728.